Available online at www.sciencedirect.com
ScienceDirect
Trans. Nonferrous Met. Soc. China 29(2019) 1753−1762
Transactions of Nonferrous Metals Society of China
www.tnmsc.cn

Online evaluation of electroless deposition rate by electrochemical noise method

Z. RAJABALIZADEH, D. SEIFZADEH, A. HABIBI-YANGJEH

Applied Chemistry Department, Faculty of Science, University of Mohaghegh Ardabili, Ardabil, Iran

Received 25 November 2018; accepted 18 June 2019

Abstract: Continuous noise resistance calculation (CNRC) technique was used for online determination of the electroless nickel deposition rate on zirconium pretreated magnesium alloy. For this purpose, the noise resistance (R_n) variation with time was calculated for the pretreated alloy surface in the electroless plating solution. The CNRC results were described by energy dispersive X-ray spectroscopy (EDS) and scanning electron microscopy (SEM) techniques. Also, potentiodynamic polarization and gravimetric measurements were used for determination of the electroless deposition rate at the same time period and the results were compared with the CNRC results. The R_n variation with plating time shows that the electroless plating consists of different stages with various deposition rates. The results of the CNRC and polarization methods were not in acceptable agreement due to the limitations of the polarization method for online monitoring of the deposition rate. However, the results of the gravimetric measurements were in complete agreement with the CNRC technique and so, the CNRC can be considered as suitable tool for online evaluation of the electroless deposition rate.

Key words: magnesium alloy; electroless plating; deposition rate; electrochemical noise; SEM; EDS

1 Introduction

Electroless plating is becoming a pervasive technique used in surface finishing industries to protect, repair and enhance the life of the metal components. In spite of some surface treating methods which are in the early stage of the research, the electroless plating has become a commercial process with widespread applications in various industries [1−7]. Certainly, the main purpose of the electroless plating on metals is to improve the most important properties such as corrosion resistance, wear resistance, and hardness. Properties of the electroless coating are affected by some variables such as operation condition, bath composition, temperature, pH, and nature of the substrate [8−13]. The electroless deposition rate is another important parameter that should be controlled to obtain the desired coating. The effect of various parameters on the electroless plating rate has been previously investigated [14−18]. Generally, the rate of the electroless plating is determined by polarization [19], gravimetry [20], and electrochemical quartz crystal microbalance (EQCM) [21] methods. The polarization method is an electrochemical concept which is able to determine the rate of redox reactions at the electrode/solution interface. This method is based on the external DC perturbation of working electrode in test solution. Due to the electrochemical nature of the electroless plating, polarization measurement can be used for the deposition rate estimation. However, application of the external perturbation, especially in the case of active metals such as magnesium and its alloys leading to severe oxidation of the substrate during the anodic polarization. This method is mainly used for determining instantaneous deposition rate. However, it should be considered that the polarization test, depending on the scan rate of the potential, takes some minutes, which causes unwanted errors because the deposition rate may be changed during the measurement period. Furthermore, this method is not suitable for continuous monitoring of the plating rate since it requires frequent polarization measurements at different time and inevitably using different test samples. Also, this kind of measurement is time-consuming and the extracted data are not completely reliable.

Gravimetric measurement is the most conventional, simple, and accurate method for the plating rate determination. However, the sensitivity of the mass

Corresponding author: D. SEIFZADEH; Tel: +98-4533514702; Fax: +98-4533514701; E-mail: Seifzadeh@uma.ac.ir, dseyfzadeh@yahoo.com
DOI: 10.1016/S1003-6326(19)65083-1

measurement is low in the beginning plating time due to the low mass gain. Furthermore, this technique is done ex-situ and so, the calculated deposition rate is the average mass gain of the sample divided by the plating time and surface area at a certain time period not in each desired plating time. In other words, this method is not suitable for online monitoring of the plating rate, too.

Among the above-mentioned methods, EQCM is the only method capable of in-situ measuring of the plating rate. However, EQCM data are not fully reliable because the plating rate values in this method are based on the mass change of the quartz crystal, so the effect of the substrate on the plating rate is neglected. In other words, the deposition rate on the quartz crystal will be different from the real substrates, such as steel and magnesium. Moreover, EQCM is not economical due to the high price of the equipment.

According to the above-mentioned discussion, it is necessary to introduce a simple, accurate, nondestructive, and cost-effective method for in-situ monitoring of the electroless plating rate. Electrochemical noise (EN) technique is based on the measurement of current and potential fluctuations in the electrochemical systems [22]. Although, this technique is widely used within the corrosion engineering as a helpful process monitoring tool but it could be also useful in the determination of the mechanism and kinetics of other electrochemical processes like as the electroless plating. In fact, kinetic and mechanism of the plating reaction can be studied by the electrochemical noise method as like as the corrosion process since both of them can be explained by the mixed potential theory.

In this work, the mechanism and deposition rate of the electroless nickel plating on the zirconium pretreated AM60B magnesium alloy were evaluated by continuous noise resistance calculation (CNRC) technique [23] as a unique analysis method of the electrochemical noise measurement. Also, two classic methods namely potentiodynamic polarization and gravimetry were used to determine the mechanism and deposition rate to compare the results. Furthermore, scanning electron microscopy (SEM) and energy dispersive X-ray spectroscopy (EDS-mapping) techniques were used for description of the EN results and determining the mechanism of the plating process.

2 Experimental

2.1 Substrate and plating

In this work, AM60B magnesium alloy with dimensions of 1 cm × 2 cm × 0.5 cm was used as the substrate. The test samples were cleaned and pretreated in H_2ZrF_6 solution and then were immersed in the electroless bath for studying the kinetic and mechanism of the plating process. The chemical composition of the alloy and more details of the pretreatment process were mentioned in our recent study [24]. The electroless plating bath composition is presented in Table 1. The electroless plating rate along with the morphology and chemical composition of the resultant coating can be affected by the stirring rate [25] but, no stirring was used in this work.

Table 1 Bath composition and operation condition of electroless plating

Bath composition	Concentration	Condition
$NiSO_4·6H_2O$ (Merck, 99%)	15 g/L	Temperature: 65 °C
$NaH_2PO_2·H_2O$ (Loba chemie, 99%)	14 g/L	pH= 6.4
$NaC_2H_3O_2$ (Merck, >99.5%)	13 g/L	Volume: 100 mL for each sample
NH_4HF_2 (Loba chemie, 98%)	8 g/L	
HF (Loba chemie, 40% v/v)	12 mL/L	
NH_3 for pH adjusting (Rankem, 30%)	–	
Thiourea (Merck, extra pure)	1×10^{-6}/(g·L^{-1})	

2.2 Electrochemical noise measurement

The CNRC technique [24] was used to determine the in-situ electroless nickel plating rate on zirconium pretreated magnesium alloy. The electrochemical noise data were recorded using an Autolab (PGSTAT30) Potentiostat/Galvanostat instrument and GPES (version 4.9005 Beta) software. Two identical zirconium pretreated samples were used as dual working electrodes (with 1 cm^2 exposed surface area) and a saturated Ag/AgCl electrode as a reference electrode. The EN measurements as like as the gravimetric and polarization tests were done in the electroless plating bath. In other words, the EN measurements were recorded immediately after the immersion of the zirconium pretreated alloy substrate in the electroless plating bath. For this purpose, electrochemical current noise (ECN) between two working electrodes and simultaneously, electrochemical potential noise (EPN) fluctuations were measured with respect to the reference electrode. The sampling interval time was 0.5 s over 8192 data point and accordingly, the frequency domain [26] was from 1 Hz to 0.24 mHz. Before the online evaluation of the noise resistance (R_n) in the plating period, DC trend was removed from the raw ECN and EPN data by moving average removal (MAR) method according to ASHASSI-SORKHABI et al [26] with p value of 3. The R_n values ($R_n=\sigma(v(t))/\sigma(I(t))$) were calculated by the CNRC technique with p value of 20 after DC trend removal and the measurement was

repeated 3 times. DC trend removal and calculation of the R_n were done using MATLAB 8.3 software.

2.3 Surface characterization

Surface morphology of the electroless plated nickel coatings at different immersion time (30, 60, 90, 200, 900, 1500, 2500, and 3600 s) was observed by SEM (LEO, VP 1430). Moreover, EDS-mappings (RONTEC Gmbh, Germany) of the coating after 90, 2200 and 3600 s plating time were performed to display the elemental distribution. Line profile of the nickel coating from the cross section view was recorded by FESEM device (MIRA3 TESCAN-XMU).

2.4 Polarization measurements

The potentiodynamic polarization measurements were conducted using μAutolab3 Potentiaostat/ Galvanostat instrument and NOVA (version 1.6) computer program. The zirconium pretreated alloy specimens (1 cm^2) were used as the working electrode while a platinum sheet (1 cm^2) and a saturated Ag−AgCl electrode were used as the auxiliary and reference electrodes, respectively. In order to execute the polarization examinations, the Zr pretreated alloy samples were immersed in the electroless plating solution at different time (0, 900, 1800, 2700, 3600 s) and the potential of the working electrodes swept from cathodic to anodic direction with a scan rate of 1 mV/s. A fresh sample was used for each immersion time and the polarization test was repeated 5 times and the results were averaged. The time duration for each polarization test was about 15 min.

2.5 Gravimetrical method

The mass difference of plated alloy samples was measured by an electronic balance (Sartorius, Germany) with accuracy of ±0.0001 g in order to calculate the electroless plating rate. The electroless plating was done for the different time (30, 60, 90, 200, 900, 1500, 2200, 3000, and 3600 s) to determine the mass changes of the sample before and after the plating. The plating rate v (μm/h) can be calculated as a function of mass changes as follows:

$$v=\frac{(m_t-m_o)\times10^4}{\rho At} \tag{1}$$

where m_t, m_o, ρ, A, and t are mass of the plated sample for time t (g), mass of the sample after the conversion coating (g), density of nickel (8.9 g/cm^3), surface area of the sample (cm^2), and deposition time (h), respectively. This test was repeated for 3 times in the case of each immersion time and the results were averaged.

3 Results and discussion

3.1 EN measurement

EPN and ECN data were recorded to determine the electroless plating rate, mechanism of nucleation, and growth of nickel particles on zirconium pretreated magnesium alloy substrate. Figure 1 shows the typical raw and trend removed EPN and ECN data.

The R_n variation with time is calculated by the CNRC technique and the results are represented in Fig. 2. The R_n variations with time consist of some raisings and fallings due to the different kinetics of nucleation and growth steps which will be discussed in detail. As it was mentioned in the introduction section, the electroless plating could be described by the mixed potential theory. Therefore, in the electroless plating as like as the corrosion process, the resistance at the electrode/ electrolyte interface is inversely proportional to the deposition rate. As it is clear from Fig. 2, during the first stage of the immersion (from start point to about 200 s) the R_n values are considerably high. These high values of R_n in the early stage of the immersion probably demonstrate the low deposition rate, which is due to the incubation stage before the nickel nuclei began to grow. Incubation stage could be introduced as the time period from the contact of the plating solution with the substrate to the start of the electroless plating reaction (reduction of nickel ions by hypophosphite). In other words, incubation time can be defined as the minimum time required for activation of the electroless process. It has been previously approved that the incubation time mainly depended on the type of the plated surface and its pretreatment [27]. In this work, the incubation period is short enough (maximum 200 s), indicating that the zirconium conversion coating acts as a suitable pretreatment for application of the Ni−P coating on AM60B alloy.

It should be mentioned that the magnesium alloy can be corroded in the plating solution at initial stage of the immersion due to the inherent tendency of magnesium to react with the aqueous environment. In other words, corrosion and electroless deposition are two simultaneous competitive reactions at initial immersion [2,28]. So, the calculated R_n values are not only related to the plating process at the beginning of the electroless plating. In this situation, it is clear that certain discussion about the plating rate is impossible since the high values of the R_n at initial immersion may be related not only to the low deposition rate (as mentioned above), but also due to the low corrosion rate of the alloy substrate. This fact may influence not only the CNRC results but also the results of any plating rate monitoring methods including gravimetric or other electrochemical

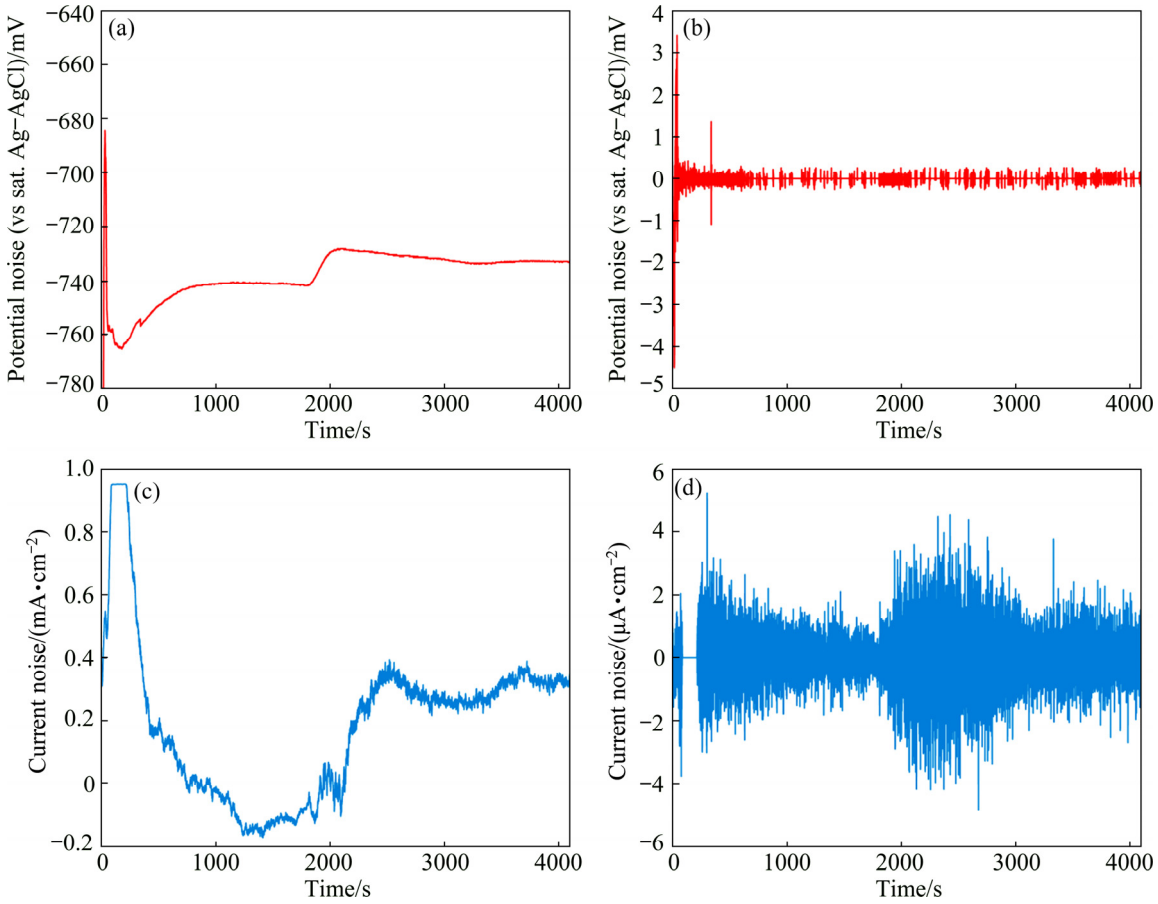

Fig. 1 Raw and trend removed EPN (a, b) and ECN (c, d) data recorded in electroless plating bath

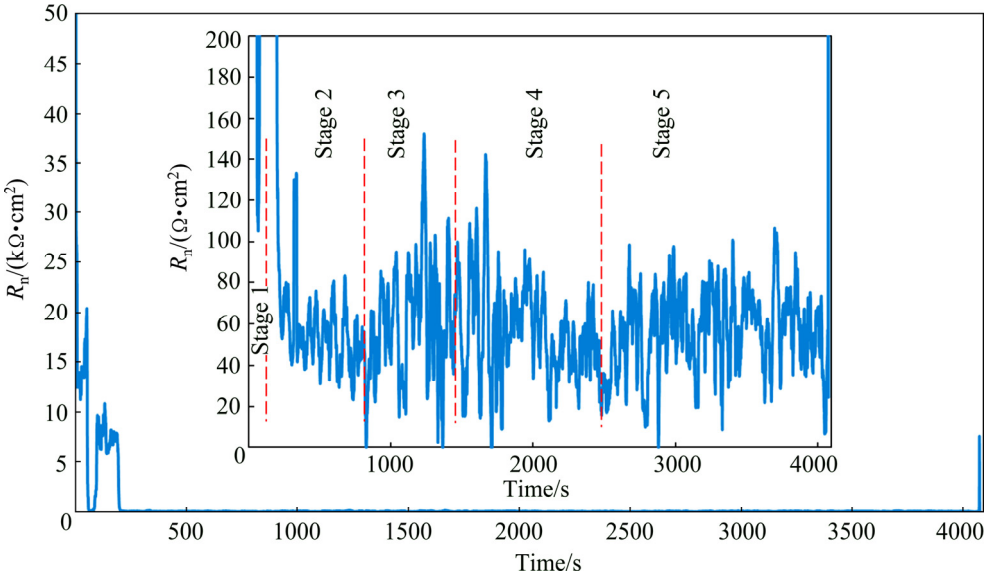

Fig. 2 Variation of noise resistance (R_n) with time

methods. However, this problem is gradually removed by extending the plating time and covering of the alloy surface by the first coating layer. In other words, the influence of magnesium corrosion was just limited to the beginning plating before the alloy substrate was covered by the electroless coatings [13].

Corresponding SEM images are shown in Fig. 3 to confirm the nucleation and growth of nickel particles. The SEM image of the zirconium conversion layer on the substrate (Fig. 3(a)) displayed that the surface was covered by an island-like microstructure. The formation mechanism of this layer was discussed elsewhere in

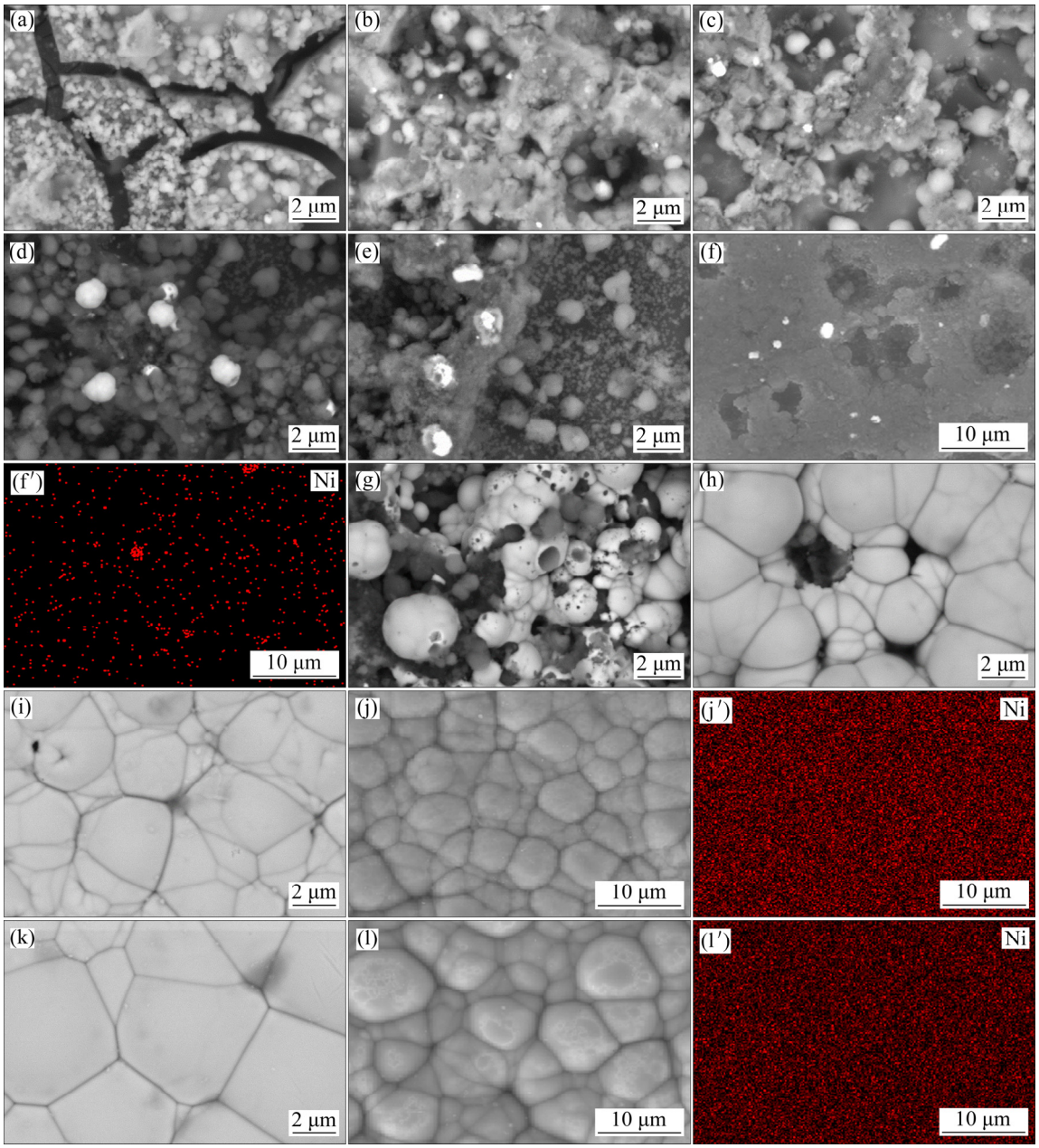

Fig. 3 SEM images after Zr pretreatment (a) and 30 s (b), 60 s (c), 90 s (d), and 200 s (e) plating; EDS-maps after 90 s plating (f, f′); SEM images after 900 s (g), 1500 s (h), and 2500 s (i) plating; EDS-maps after 2500 s (j, j′); SEM image after 3600 s (k) plating; and EDS-maps after 3600 s (l, l′) plating

detail [24,29,30]. The surface morphologies of the sample after 30 and 60 s immersion are shown in Figs. 3(b) and (c), respectively. Comparison of the morphological image in Fig. 3(a) with Figs. 3(b) and (c) shows that the initial growth of the electroless deposited nickel coating in the incubation stage takes place through the cracks of the zirconium conversion layer. After immersion of the substrate in the electroless bath, nickel ion reduction is thermodynamically possible but it cannot take place due to the low kinetics [31]. Immediately after immersion of the magnesium substrate in the bath, magnesium dissolves to Mg^{2+} in the acidic electroless bath. After that, replacement reaction occurs between nickel ions and magnesium atoms to form the initial nickel particles on the surface. Then, with the catalytic support, the overvoltage of the electroless process removes and the deposition proceeds. In the SEM images of the surface after about 90 and 200 s immersion (Figs. 3(d) and (e)), the number of the nucleation centers was increased dramatically due to the passing of the plating time. Furthermore, the EDS-mapping of the sample after 90 s immersion (Fig. 3(f, f′)) was performed to confirm the above-mentioned mechanism. The SEM image after 90 s (corresponding to the EDS-mapping

image) is shown again in Fig. 3(f) because the different instrument was used for the EDS-mapping analysis. The EDS-mapping of the sample after 90 s immersion shows that nickel nuclei are distributed over the surface. Some areas which seem brighter in SEM and EDS-mapping images are related to the growing nickel grains. Regarding to the noise data and SEM images, by increasing the number of nucleation centers on the surface, the R_n value decreased (from about 20000 to less than 10000 Ω·cm^2). Therefore, stage 1 in Scheme 1 is related to the starting of the nucleation and increasing of the nucleation centers on the surface mostly by the replacement reaction.

In the second stage (between about 200 to 900 s immersion), the noise resistance was decreased dramatically to less than 100 Ω·cm^2 indicating a drastic increase in the rate of nickel ions reduction. This result can be related to simultaneous growth of earlier formed nickel nuclei (through the autocatalytic electroless process) and appearance of new nucleation centers which can be seen in Fig. 3(g) [32]. Thus, stage 2 in Scheme 1 is mainly related to the starting of the electroless plating through the autocatalytic reduction of nickel by hypophosphite.

In the third stage (between about 900 to 1500 s immersion), compared with the last time period, R_n was relatively increased and so the plating rate was decreased. This is probably related to the fact that the alloy surface gradually covers by the first layer of the Ni−P coating at plating time higher than 900 s due to the initial nuclei growing and so, further propagation of the electroless process needs new nucleation on top of the already deposited layer. The nucleation centers in the first stage form by the replacement reaction while the nucleation centers of this stage form by the autocatalytic deposition [13,33,34]. The SEM image in Fig. 3(h) displays that the further deposition proceeds by growth of the newly formed nickel nuclei in this time period. So, stage 3 in Scheme 1 is mainly related to the formation of secondary nucleation centers on the primarily formed nickel film and synchronic growth of the grains.

In the fourth stage (between about 1500 to 2500 s immersion), the R_n decreased again and the deposition rate increased due to the crystallization of the secondary nucleation centers which were created at the last stage. The complete coverage of the surface and formation of cauliflower-like morphology after about 2500 s electroless plating can be observed in Fig. 3(i). The EDS-mapping after about 2500 s immersion (Fig. 3(j, j′)) showed that nickel atoms distributed all over the surface, which confirms complete coverage of the alloy surface by the Ni−P coating. Therefore, stage 4 in Scheme 1 is related to the growth of the secondary nucleation centers to form the second layer of the electroless coating.

In the fifth stage (between about 2500 s to the end of the immersion), R_n (and subsequently deposition rate) reached almost constant value. The SEM (Fig. 3(k)) and related EDS-mapping (Fig. 3(l, l′)) images show that the

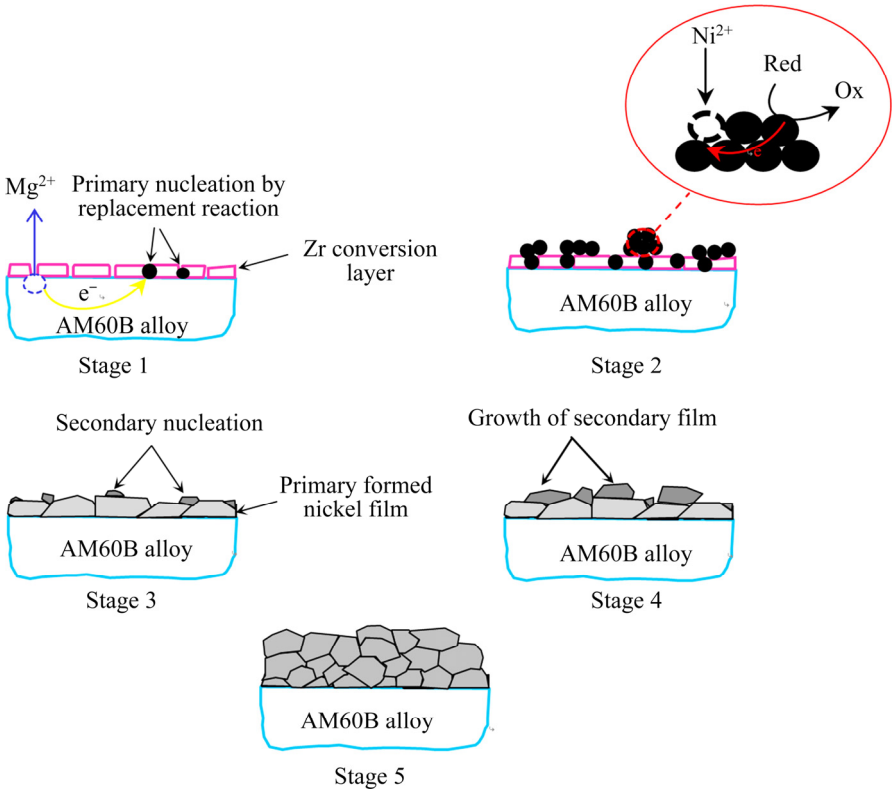

Scheme 1

surface was covered by the electroless coating. This may be due to the decreasing of the competition between secondary layer nucleation and growth of them. Generally, at the stage 5 in Scheme 1, the nickel coating with an equiaxed microstructure was formed due to the formation of randomly oriented crystals [34].

The line profile of the electroless coating on AM60B magnesium alloy from the cross-section view after about 3600 s plating (Fig. 4) showed the variation of Ni, Cu, and P elements from the substrate/coating interface to the outer surface of the coating. The moderate amount of P along the line profile of the coating (about 6 wt.%) confirms that the coating has mixed crystalline-amorphous microstructure. The deposition of Ni and P in the electroless plating could be explained by the following reactions [24]:

$$2H_2PO_2^- + 2H_2O + Ni^{2+} \rightarrow Ni + 2H^+ + 2H_2PO_3^- + H_2 \quad (2)$$

$$2H_2PO_2^- + 6H^- + 4H_2O \rightarrow 2P + 5H_2 + 8OH^- \quad (3)$$

Moreover, the averaged amount of Cu in the coating was about 2 wt.% which is attributed to its co-deposition through the following reaction [35]:

$$Cu^{2+} + 2H_2PO_2^- + H_2O \rightarrow Cu + 2H_2PO_3^- + 2H^+ + H_2 \quad (4)$$

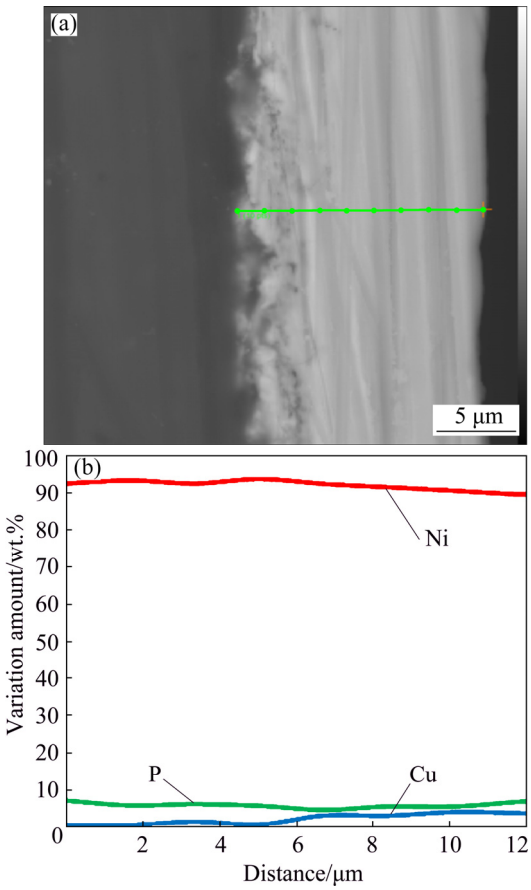

Fig. 4 Cross-section view (a) and EDS-line profile (b) of electroless Ni−P coating

Furthermore, it is clear that the nickel coating has mechanically interlocked to the substrate and has about 15 μm in thickness after 3600 s immersion.

3.2 Polarization measurements

As a classic electrochemical method, potentiodynamic polarization technique was used to monitor the plating rate and the extracted results were compared with those obtained by the EN measurements. The polarization curves of the zirconium pretreated samples after various immersion time in the plating bath are typically shown in Fig. 5.

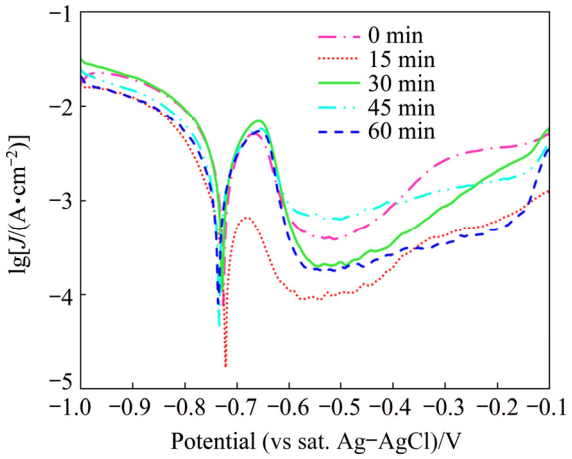

Fig. 5 Potentiodynamic polarization curves after various immersion time in plating bath

The polarization curves were analyzed by Tafel extrapolation technique and the obtained results including Tafel slopes, mixed potential (φ_{mixed}) of the sample, and deposition current density (J_{dep}) are listed in Table 2. It should be mentioned that each extracted polarization parameter was calculated by averaging the results of 5 different repetitions.

Table 2 Polarization parameters of samples after different immersion time in plating bath

Plating time/s	b_a/ (mV·dec^{-1})	b_c/ (mV·dec^{-1})	φ_{mixed} (vs sat. Ag−AgCl)/V	J_{dep}/ (mA·cm^{-2})
0	137	135	−0.728	2.148
900	132	159	−0.732	2.300
1800	125	144	−0.732	2.572
2700	118	178	−0.735	2.393
3600	139	142	−0.734	2.603

Since the deposition current density is directly proportional to the deposition rate, its changes with the plating time are shown in Fig. 6. Comparison of the obtained results with the results of the EN measurements (Fig. 2) shows that there is not acceptable agreement between these two methods. Despite using the

polarization as a conventional method in the deposition rate measurement, this method has some disadvantageous which were mentioned in the introduction section and will be discussed here in details. Because of the external perturbation during the polarization test, the plating does not take place in the open circuit potential (OCP). In fact, nickel ions reduction and hypophosphite ions oxidation accelerate with respect to the freely plating or OCP condition under the cathodic and anodic polarization, respectively. In addition, continuous monitoring of the deposition rate is not possible by the polarization test. As it is clear from Fig. 6, J_{dep} variation with time consists of only five separate data points. In other words, determination of the deposition rate is not possible in each desired time because each polarization test lasts about 15 min and necessarily, the test was carried out only in some specific time. So, the polarization tests were performed immediately after immersion of the pretreated substrate in the electroless bath and then after immersion for 900, 1800, 2700, and 3600 s by using separate samples.

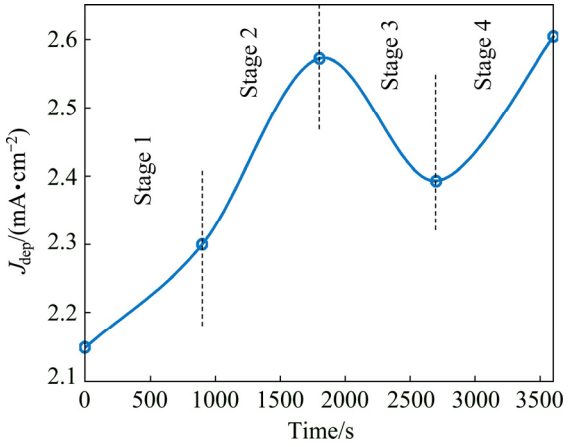

Fig. 6 Variation of J_{dep} versus immersion time in plating solution

The J_{dep} variation (Fig. 6) over the test time consists of four different stages. At the first stage, (between 0 and 900 s) the J_{dep} value (and consequently the deposition rate) was increased. Comparison of the R_n values (stages 1 and 2 in Fig. 2) and the J_{dep} (stage 1 in Fig. 6) shows that the deposition rate increases at both of them but the very low deposition rate of the sample in the early stage of the immersion (between start point and about 200 s immersion) in EN measurements is not detectable by the polarization tests.

At the second stage (between 900 and 1800 s), the deposition rate increased sharply while the EN measurement showed that the deposition rate decreased between about 900 and 1500 s and then increased. In fact, decreasing of the deposition rate between 900 and 1500 s immersion was not observed with the polarization method due to its limitation for online monitoring of the deposition rate in each desired time as mentioned above.

At the stages 3 (between 1800 and 2700 s) and 4 (between 2700 and 3600 s) in Fig. 6, there was no trend agreement between the polarization and EN measurements, which may be attributed to the limited data points in the polarization test. Moreover, obvious passivation behavior was observed at the anodic branch of the polarization curves which complicated the anodic Tafel behavior. So, accurate calculation of the anodic Tafel slopes (and subsequently the J_{dep}) is not possible leading to unwanted errors in the polarization measurements.

3.3 Gravimetric measurement

Gravimetric measurement as a conventional and accurate method was used for validation of the EN results in determination of the plating rate. The immersion time for the gravimetric measurements was chosen according to the R_n variation and the obtained results are shown in Fig. 7. The negative values of the deposition rate at the beginning of plating (between the start point and about 500 s) are due to the dissolution of magnesium in the plating bath. In fact, the pretreated alloy sample loses mass due to the corrosion of the magnesium in the first moments of the immersion in the plating bath. Therefore, it seems that the corrosion process (simultaneous dissolution of magnesium and reduction of water) is predominant to both replacement reaction between nickel ions and magnesium substrate (nucleation process) and autocatalytic (electroless) reduction of nickel by hypophosphite. As it is clear, there is a relatively good trend agreement between the gravimetric results and the EN data since the deposition rate variation between each immersion period is relatively as same as the EN results. So, it can be concluded that the CNRC is a suitable technique for in-situ monitoring of the electroless deposition rate.

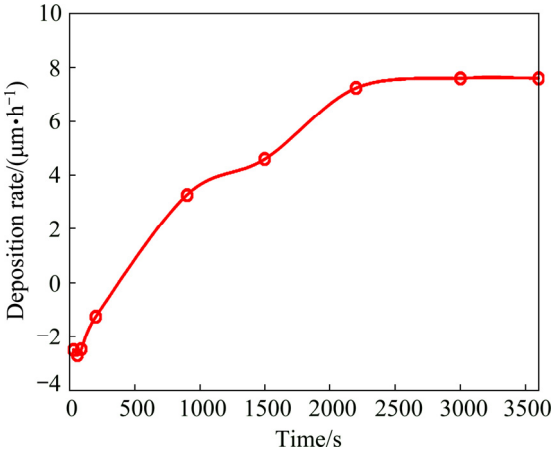

Fig. 7 Deposition rate of electroless nickel plating versus time

4 Conclusions

(1) The R_n variation with time shows that the electroless coating process on the magnesium alloy consists of different stages. At the early stage of the immersion (before 200 s), the values of the R_n are high due to the low number of nucleation centers. At this stage, the nucleation starts via the replacement reaction between magnesium atoms and nickel ions. However, after starting the electroless plating (after about 200 s), the R_n decreases and the plating rate increases. After the primary nucleation, the growth of the nuclei starts to cover the surface and an increase takes place in R_n values due to the different kinetics of the nucleation and growth. By proceeding of the electroless plating and covering of the surface by the first layer of nickel, the secondary nucleation centers form on the primarily formed layer and the R_n decreases. At the end of the immersion, the R_n reaches the constant value and the plating proceeds to thicken the coating.

(2) The SEM and EDS-mapping techniques confirmed the EN results and formation mechanism of the electroless nickel plating.

(3) The results of the polarization and EN measurements were compared and it was found that there is not an acceptable agreement due to some limitations with the polarization method.

(4) The results of the gravimetric measurements for determining of the plating rate were in complete agreement with the EN results.

References

[1] XIE Zhi-hui, SHAN Shi-yao. Nanocontainers-enhanced self-healing Ni coating for corrosion protection of Mg alloy [J]. Journal of Materials Science, 2018, 53: 3744−3755.

[2] RAJABALIZADEH Z, SEIFZADEH D. Application of electroless Ni−P coating on magnesium alloy via CrO_3/HF free titanate pretreatment [J]. Applied Surface Science, 2017, 422: 696−709.

[3] BOSTANI B, PARVINI AHMADI N, YAZDANI S, ARGHAVANIAN R. Co-electrodeposition and properties evaluation of functionally gradient nickel coated ZrO_2 composite coating [J]. Transactions of Nonferrous Metals Society of China, 2018, 28: 66−76.

[4] ZHANG Xiang-zhao, WU Xiao-lang, LIU Gui-wu, LUO Wen-qiang, GUO Ya-jie, SHAO Hai-cheng, QIAO Guan-jun. Wetting of molten Sn−3.5Ag−0.5Cu on Ni−P(−SiC) coatings deposited on high volume faction SiC/Al composite [J]. Transactions of Nonferrous Metals Society of China, 2018, 28: 1784−1792.

[5] HESHMATI M, SEIFZADEH D, SHOGHI P, GHOLIZADEH-GHESHLAGHI M. Duplex Ni−Zn−Cu−P/Ni−P electroless coating on magnesium alloy via maleic acid pretreatment [J]. Surface and Coatings Technology, 2017, 328: 20−29.

[6] FANG Meng, HU Ling, YANG Lei, SHI Chang-dong, WU Yu-cheng, TANG Wen-ming. Electroless plating and growth kinetics of Ni−P alloy film on SiC_p/Al composite with high SiC volume fraction [J]. Transactions of Nonferrous Metals Society of China, 2016, 26: 799−805.

[7] BALARJU J N, SANKARA NARAYANAN T S N, SESHADRI S K. Structure and phase transformation behaviour of electroless Ni−P composite coatings [J]. Materials Research Bulletin, 2006, 41: 847−860.

[8] YUCHENG W, RONG R, FENGTAO W, ZAOSHI Y, TUGEN W, XIAOYE H. Preparation and characterization of Ni−Cu−P/CNTs quaternary electroless composite coating [J]. Materials Research Bulletin, 2008, 43: 3425−3432.

[9] ZHANG X, HAN W, FAN D, ZHENG Y. Electroless iron plating on pure magnesium for biomedical applications [J]. Materials Letters, 2014, 130: 154−156.

[10] CUI X, JIN G, LI Q, YANG Y, LI Y, WANG F. Electroless Ni−P plating with a phytic acid pretreatment on AZ91D magnesium alloy [J]. Materials Chemistry and Physics, 2010, 121: 308−313.

[11] WANG Hui-long, LIU Ling-yun, JIANG Wen-feng. Effect of novel ternary ligand system on acidic electroless Ni−P plating on AZ91D magnesium alloy [J]. Transactions of Nonferrous Metals Society of China, 2014, 24: 3014−3022.

[12] ASHASSI-SORKHABI H, RAFIZADEH S H. Effect of coating time and heat treatment on structures and corrosion characteristics of electroless Ni−P alloy deposits [J]. Surface and Coatings Technology, 2004, 176: 318−326.

[13] QIN Tie-nan, MA Li-qun, YAO Yan, NI Cong, ZHAO Xiang-yu, DING Yi. An in situ measure method to study deposition mechanism of electroless Ni−P plating on AZ31 magnesium alloy [J]. Transactions of Nonferrous Metals Society of China, 2011, 21: 2790−2797.

[14] YAN M, YING H G, MA T Y, LUO W. Effects of Yb^{3+} on the corrosion resistance and deposition rate of electroless Ni−P deposits [J]. Applied Surface Science, 2008, 255: 2176−2179.

[15] WU L, YANG Z, QIN G. Kinetic study of a novel electroless NiP deposition on AZ91D magnesium alloy using nickel hypophosphite as the metal salt [J]. Journal of Alloys and Compounds, 2017, 694: 1133−1139.

[16] BASKARAN I, SANKARA NARAYANAN T S N, STEPHEN A. Effect of accelerators and stabilizers on the formation and characteristics of electroless Ni−P deposits [J]. Materials Chemistry and Physics, 2006, 99: 117−126.

[17] ASHASSI-SORKHABI H, MIRMOHSENI A, HARRAFI H. Evaluation of initial deposition rate of electroless Ni−P layers by QCM method [J]. Electrochimica Acta, 2005, 50: 5526−5532.

[18] MATSUBARA H, YONEKAWA T, ISHINO Y, SAITO N, NISHIYAMA H, INOUE Y. The observation of the nucleation and growth of electrolessly plated nickel deposited from different bath pH by TEM and QCM method [J]. Electrochimica Acta, 2006, 52: 402−407.

[19] ASHASSI-SORKHABI H, MORADI-HAGHIGHI M, HOSSEINI M G. Effect of rare earth (Ce, La) compounds in the electroless bath on the plating rate, bath stability and microstructure of the nickel-phosphorus deposits [J]. Surface and Coatings Technology, 2008, 202: 1615−1620.

[20] XU H, BRITO J, SADIK O A. Mechanism of stabilizer acceleration in electroless nickel at wirebond substrates [J]. Journal of Electrochemical Society, 2003, 150: 816−822.

[21] SARGENT A, SADIK O A. Probing the mechanism of electroless gold plating using an EQCM: II. Effect of bath additives on interfacial plating processes [J]. Journal of Electrochemical Society, 2001, 148: 413−420.

[22] SEIFZADEH D, BEZAATPOUR A, ASADPOUR JOGHANI R. Corrosion inhibition effect of N, N′-bis (2-pyridylmethylidene)-1, 2-diiminoethane on AZ91D magnesium alloy in acidic media [J]. Transactions of Nonferrous Metals Society of China, 2014, 24: 3441−3451.

[23] TAN Y, BAILEY S, KINSELLA B. Studying the formation process of chromate conversion coatings on aluminium using continuous electrochemical noise resistance measurements [J]. Corrosion Science, 2002, 44: 1277−1286.
[24] RAJABALIZADEH Z, SEIFZADEH D, HABIBI-YANGJEH A, MESRI GUNDOSHMIAN T, NEZAMDOUST S. Electrochemical noise analysis to examine the corrosion behavior of Ni−P deposit on AM60B alloy plated by Zr pretreatment [J]. Surface and Coatings Technology, 2018, 346: 29−39.
[25] KALANTARY M R, HOLBROOK K A, WELLS P. B. Optimisation of a bath for electroless plating and its use for the production of nickel−phosphorus−silicon carbide coatings [J]. Transactions of the IMF, 1993, 71: 55−61.
[26] ASHASSI-SORKHABI H, SEIFZADEH D, HOSSEINI M G. EN, EIS and polarization studies to evaluate the inhibition effect of 3H-phenothiazin-3-one, 7-dimethylamin on mild steel corrosion in 1 M HCl solution [J]. Corrosion Science, 2008, 50: 3363−3370.
[27] FLIS J, DUQUETTE D J. Catalytic activity of iron, nickel, and nickel−phosphorus in electroless nickel plating [J]. Journal of Electrochemical Society, 1984, 131: 34−39.
[28] RONCEVIC I S, BUZUK M, VLADISlAVI N. Effective and environmentally friendly nickel coating on the magnesium alloy [J]. Metals, 2016, 6: 316−331.
[29] YI A, DU J, WANG J, MU S, ZHANG G, LI W. Preparation and characterization of colored Ti/Zr conversion coating on AZ91D magnesium alloy [J]. Surface and Coatings Technology, 2015, 276: 239−247.
[30] LIU Z, JIN G, SONG J, CUI X, CAI Z. Remanufacture of zirconium based conversion coatings on the surface of magnesium alloy [J]. Journal of Materials Engineering and Performance, 2017, 26: 1776−1783.
[31] DELAUNOIS F, PETITJEAN J P, LIENARD P, JACOB-DULIERE M. Autocatalytic electroless nickel−boron plating on light alloys [J]. Surface and Coatings Technology, 2000, 124: 201−209.
[32] SVIRIDOV V V, GAEVSKAYA T V, STEPANOVA L I, VOROBYOVA T N. Electroless deposition and electroplating of metals [M]. Minsk: Belarusian State University, 2003.
[33] SEIFZADEH D, KAZEMI MOHSENABADI H, RAJABALIZADEH Z. Electroless Ni−P plating on magnesium alloy by innovative, simple and non-toxic oxalate pretreatment and its corrosion protection [J]. RSC Advances, 2016, 6: 97241−97252.
[34] SCHULTZE J W, OSAKA T, DATTA M. Electrochemical microsystem technologies [M]. United State: CRC Press, 2002.
[35] RAJABALIZADEH Z, SEIFZADEH D. The effect of copper ion on microstructure, plating rate and anticorrosive performance of electroless Ni−P coating on AZ61 magnesium alloy [J]. Protection of Metals and Physical Chemistry of Surfaces, 2014, 50: 516−523.

电化学噪声法在线评估化学沉积速率

Z. RAJABALIZADEH, D. SEIFZADEH, A. HABIBI-YANGJEH

Applied Chemistry Department, Faculty of Basic Science, University of Mohaghegh Ardabili, Ardabil, Iran

摘　要：采用连续噪声电阻计算(CNRC)技术在线测定经锆预处理后镁合金的化学镀镍速率。为此，计算化学镀液中预处理合金表面的噪声电阻(R_n)随时间的变化。采用能量色散 X 射线谱仪(EDS)和扫描电镜(SEM)技术对 CNRC 结果进行解释。同时，用动电位极化法和重量法测定同一时间区间内的化学沉积速率，并与 CNRC 结果进行比较。R_n 随施镀时间的变化表明，化学镀是由具有不同沉积速率的几个阶段组成的。由于极化法在线监测沉积速率的局限性，CNRC 结果和极化法的结果并不一致。然而，重量法的结果与 CNRC 结果完全一致。因此可以认为 CNRC 是一种合适的化学沉积速率在线评估工具。

关键词：镁合金；化学镀；沉积速率；电化学噪声；SEM；EDS

(Edited by Xiang-qun LI)